Geophysical Research Letters

RESEARCH LETTER
10.1029/2024GL111831

Importance of Longwave Radiative Forcing by Icy Clouds in Maintaining Miocene High-Latitude Warmth

Xiaoqing Liu[1], Ashley Griffin[2], Muge Komurcu[3], and Matthew Huber[1]

[1]Department of Earth, Atmospheric and Planetary Sciences, Purdue University, West Lafayette, IN, USA, [2]Joint Center for Satellite Data Assimilation, University Corporation for Atmospheric Research, Boulder, CO, USA, [3]Department of Earth, Atmospheric and Planetary Sciences, Massachusetts Institute of Technology, Cambridge, MA, USA

Key Points:

- Modifying ice nucleation and cloud phase partitioning schemes in Miocene simulations increases ice cloud amounts and cloud water content
- This enhances both longwave and shortwave cloud forcing, with longwave dominating in the Arctic while they cancel out in the tropics
- The resulting higher high-latitude temperature and smaller equator-to-pole temperature gradients better match Miocene proxy reconstructions

Supporting Information:

Supporting Information may be found in the online version of this article.

Correspondence to:

X. Liu,
xiaoqingliu@purdue.edu

Citation:

Liu, X., Griffin, A., Komurcu, M., & Huber, M. (2025). Importance of longwave radiative forcing by icy clouds in maintaining miocene high-latitude warmth. *Geophysical Research Letters*, *52*, e2024GL111831. https://doi.org/10.1029/2024GL111831

Received 5 AUG 2024
Accepted 5 MAR 2025

Author Contributions:

Conceptualization: Xiaoqing Liu, Muge Komurcu, Matthew Huber
Formal analysis: Xiaoqing Liu, Ashley Griffin, Muge Komurcu
Funding acquisition: Matthew Huber
Investigation: Xiaoqing Liu, Ashley Griffin
Methodology: Xiaoqing Liu, Ashley Griffin, Muge Komurcu, Matthew Huber
Project administration: Matthew Huber
Supervision: Matthew Huber
Validation: Xiaoqing Liu, Muge Komurcu
Visualization: Xiaoqing Liu
Writing – original draft: Xiaoqing Liu

Abstract During the early-to-middle Miocene, global mean surface temperature (GMST) was approximately 8°C warmer than preindustrial, with a greater temperature increase in polar regions than the tropics. However, existing Miocene simulations underestimate this warmth, particularly in northern high latitudes. To address this discrepancy, we investigate the potential role of cloud phase. Using the Community Earth System Model, we conduct a paleoclimate sensitivity study focused on modifying ice nucleation and cloud phase partitioning schemes. These modifications increase the GMST, with a strong temperature rise in high latitudes and a muted increase in the tropics. These increases are driven by enhanced longwave cloud forcing, resulting from increased ice cloud amounts and cloud water content, and are amplified by water vapor and lapse rate feedbacks in the Arctic. Our study highlights that the improved parameterizations of cloud phase processes enhance models' capability to simulate Miocene high-latitude warmth and potentially other warm climates.

Plain Language Summary Climate models often cannot reproduce the high-latitude warmth or the small equator-to-pole temperature difference seen during the past warm periods when using CO_2 levels from proxy data. Clouds and their feedback effects have been suggested as a solution to this problem. We propose a specific hypothesis for the Miocene warmth: a detailed representation of processes affecting cloud phase results in the clouds trapping more heat from the Earth's surface (longwave radiation) and reflecting more sunlight (shortwave radiation). The heat-trapping effect is stronger than the sunlight-reflecting effect in high latitudes, causing Arctic surface warming that is further amplified by tropospheric warming and water vapor feedback. We test this idea in paleoclimate simulations with realistic Miocene settings using the Community Earth System Model (CESM) version 1.0.5. Our sensitivity test on cloud microphysics shows an increase in ice cloud amounts and cloud water content across all latitudes, resulting in a rise in global mean surface temperature relative to the standard control CESM simulation. The Arctic surface warming is most pronounced, particularly during the boreal winter, while the warming in the tropics is muted. This results in a reduced equator-to-pole surface temperature difference and diminished seasonality of Arctic surface temperatures.

1. Introduction

The early-to-middle Miocene, especially the Miocene Climate Optimum (MCO, 16.75–14.5 million years ago), represents the warmest period of the Neogene era, with the GMST ~8°C warmer than preindustrial levels (Goldner et al., 2014; Burls et al., 2021a; The Cenozoic CO2 Proxy Integration Project (CenCO2PIP) Consortium*† et al., 2023; Evans et al., 2024). During the MCO, high-latitude sea surface temperatures were 8°C–15°C warmer than modern (Shevenell et al., 2004; Super et al., 2020), while tropical regions were 2°C–6°C warmer (Holbourn et al., 2010; Sosdian & Lear, 2020; Wubben et al., 2024), leading to amplified high-latitude warmth and a weaker equator-to-pole temperature gradient compared to modern conditions. However, climate models participating in the Miocene Multi-Model ensemble (MioMIP1), driven by reconstructed CO_2 levels of 400–600 ppm (Rae et al., 2021; Sosdian et al., 2018; Steinthorsdottir, Jardine, & Rember, 2021), struggle to reproduce this warmth (Burls et al., 2021a; Goldner et al., 2014). They consistently underestimate high-latitude warmth, especially in the Northern Hemisphere, and thus overestimate equator-to-pole temperature gradients. Increasing CO_2 levels to 800–850 ppm generates better agreement with reconstructed surface temperatures, but still shows a cold bias in northern high latitudes (Burls et al., 2021a). This discrepancy occurs even when considering possible orbital forcing or permanent El Niño conditions (Goldner et al., 2014). Given that atmospheric CO_2 levels were within the range likely to be reached in the coming decades and that continental positions

Writing – review & editing: Xiaoqing Liu, Muge Komurcu, Matthew Huber

were similar to modern ones (Steinthorsdottir, Coxall, et al., 2021), understanding the drivers of the early-to-middle Miocene warmth may provide insight into future temperature changes in response to CO_2 variations.

Climate models driven by reconstructed Miocene CO_2 concentrations fail to produce amplified high-latitude warmth and reduced meridional temperature gradients. This problem is also observed for other warm periods, such as the Cretaceous (Hay et al., 2019; Niezgodzki et al., 2017), Eocene (Lunt et al., 2012, 2021), Oligocene (O'Brien et al., 2020), and mid-Pliocene (Haywood et al., 2016, 2020). Changes in ocean and atmosphere heat transport and/or vegetation inadequately explain the strong high-latitude warmth (Barron et al., 1995; Hay et al., 1997; Huber, 2012; Pagani et al., 2014). Clouds and cloud feedbacks have also been proposed to resolve this issue: for example, biological cloud feedbacks triggered by high CO_2 levels (four times preindustrial levels) have been suggested to explain Cretaceous warmth (Kump & Pollard, 2008); in the early Eocene, enhanced polar stratospheric clouds occurring under high methane (Dutta, Jucker, et al., 2023; Dutta, Sherwood, et al., 2023; Sloan & Pollard, 1998) or CO_2 levels (Kirk-Davidoff et al., 2002) have been offered as an explanation for high-latitude warmth. However, these hypotheses are less straightforward to invoke in the Miocene, because very high CO_2 or methane levels are unlikely during this period (Steinthorsdottir, Coxall, et al., 2021). Also, the magnitude of unexplained warmth (~8°C) in high latitudes is large whereas the uncertainties in forcings are smaller than those in earlier periods of Earth's history, and the Miocene ocean gateways and other boundary conditions are much closer to modern configurations despite a few key differences (Burls et al., 2021a; Steinthorsdottir, Coxall, et al., 2021).

Increased shortwave radiation due to reduced extratropical cloud albedo has been suggested as a contributor to Pliocene high-latitude warmth (Burls & Fedorov, 2014). Additionally, increased longwave warming due to changes in cloud microphysical and macrophysical properties, driven by reduced dust emissions and their effect on dust particles as ice nuclei, has been proposed to explain the mid-Pliocene high-latitude warmth (Sagoo & Storelvmo, 2017). In the Miocene, an increase in dust emission is more likely than a reduction in dust emissions (Li et al., 2011). We propose an alternative hypothesis for the Miocene by drawing on advances in our understanding of cloud phase changes and their importance for past and present climates, as well as future climate predictions. The paleoclimate response to changes in orbital parameters is sensitive to changes in the cloud phase, specifically the proportion of liquid water to ice in a cloud (Sagoo et al., 2021). Additionally, cloud feedback induced by cloud phase changes influences climate sensitivity (Frazer & Ming, 2022; Frey & Kay, 2018; Z. Li & Le Treut, 1992; McCoy et al., 2022; Mitchell et al., 1989; Tan et al., 2016; Zhao et al., 2024), representing a dominant cloud feedback at high latitudes and impacting radiative fluxes, particularly in moderately warmer climates where ice clouds are likely to be replaced by liquid clouds (Storelvmo et al., 2015). However, cloud phase processes remain inadequately represented in climate models, and there is large intermodel spread in cloud phase (Cesana et al., 2015; Komurcu et al., 2014).

We hypothesize that a better representation of processes affecting cloud phase, such as ice nucleation and growth, will increase longwave and shortwave cloud forcing (CF) across all latitudes. The total CF increase is expected to be stronger in the Arctic than in the tropics (Figure 1) due to weaker shortwave cooling effect from reduced insolation, which less effectively offsets longwave warming. This could potentially lead to significant Arctic surface warming (Figure 1), with the strongest warming occurring during the boreal winter due to the combined effects of increased longwave forcing and the absence of solar radiation. This surface warming could be amplified by tropospheric temperature and water vapor feedbacks (Abbot & Tziperman, 2008a, 2008b).

To test this hypothesis, we conduct two fully coupled paleoclimate simulations for the early-to-middle Miocene and investigate the sensitivity of high-latitude surface temperature (TS) to cloud microphysics parameterizations associated with cloud phase. In Section 2, we describe our modifications and methods; Section 3 demonstrates our results; Section 4 describes the influences of cloud properties on longwave cloud forcing, contributions from changes in water vapor and lapse rate, and the low gradient and equable climate problem; Section 5 presents conclusions and implications.

2. Methods

Two simulations were run using the Community Earth System Model version 1.0.5 (CESM1.0.5) with the Community Atmosphere Model version 5.1 (CAM5.1) (Neale et al., 2010) and the early-to-middle Miocene boundary conditions (Text S1 in Supporting Information S1) (Burls et al., 2021a; Herold et al., 2011) with 400 ppm of atmospheric CO_2. The Control simulation utilizes standard CAM5 parameterizations, and its cloud

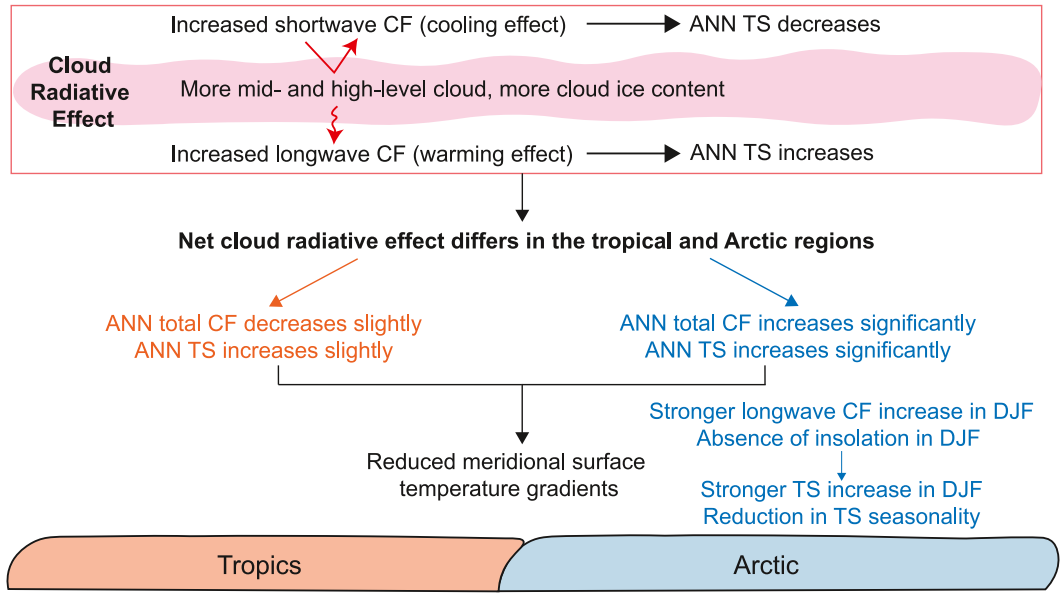

Figure 1. Schematic of Arctic and tropical cloud radiative effects and associated surface temperature changes driven by modifications in cloud phase representations made in this study. CF represents cloud forcing, ANN represents the annual mean, TS represents surface temperature, and DJF represents December–January–February. This schematic illustrates our hypothesis for addressing the Miocene low-gradient and equable climate problem.

microphysics scheme is based on Morrison and Gettelman (2008). Cloud microphysics is coupled with a three-mode version of the Modal Aerosol Module (Liu et al., 2012) to account for aerosol-cloud interactions. This model is nearly identical to the version that has had good success in simulating the Eocene and Pliocene warm climates (Feng et al., 2019; Zhu et al., 2019).

Our second simulation used a modified cloud microphysics scheme, targeting key processes like ice nucleation and cloud water phase partitioning between liquid and ice. Following DeMott et al. (2010); DeMott et al. (2015) and Storelvmo et al. (2008), we replace default parameterizations with ice nucleation and cloud phase partitioning schemes from DeMott et al. (2015) and Korolev and Mazin (2003), respectively, which have been shown to improve outcomes in contemporary simulations compared to default versions (DeMott et al., 2010, 2015; Storelvmo et al., 2008).

Ice nuclei (IN) affect ice crystal number concentrations and thus ice crystal growth and cloud water phase. Different ice nucleation schemes lead to different cloud phase (Komurcu et al., 2014) and varying levels of Arctic amplification (Tan et al., 2022). The default ice nucleation scheme in CAM5.1 (Meyers et al., 1992) uses a temperature- and ice supersaturation-dependent ice crystal activation based on mid-latitude measurements, which is not representative of observed IN behavior (Prenni et al., 2007) and does not account for model-predicted aerosol concentrations. In contrast, the modified parameterization (equation shown in Text S2 (Supporting Information S1)) based on field studies enables model-predicted aerosol concentrations to interact with cloud microphysics, generating IN concentrations that align with observations (DeMott et al., 2010, 2015). Furthermore, compared to the default scheme, the aerosol-dependent ice nucleation scheme generates a higher liquid water path in the Arctic, particularly during winter, aligning more closely with observations, as demonstrated by Xie et al. (2013).

Another modification we introduce involves the framework of cloud phase partitioning through the Wegener-Bergeron-Findeisen (WBF) process, which is characterized by ice crystals growing at the expense of surrounding cloud droplets due to the lower saturation vapor pressure of ice relative to that of liquid water. Subgrid scale variability involved in the WBF process is key to accurately modeling this process (Storelvmo et al., 2008). However, the WBF process is poorly represented in the standard CAM5. For example, CAM5 assumes unrealistic maximum overlap between ice crystals and droplets and an idealized homogeneous mixture of ice and liquid, whereas in reality, ice and liquid mix heterogeneously with separate pockets of each (Tan & Storelvmo, 2016). This leads to overestimated WBF time scales and underestimated supercooled liquid fractions in mixed-phase

clouds, which contain both liquid water (cloud droplets) and ice crystals at temperatures between −40°C and 0°C (Shupe, 2011). We replaced the default cloud phase partitioning scheme with a theoretical framework presented by Korolev and Mazin (2003). This framework was chosen because it allows for strong responses to changes in IN concentrations and provides reasonable agreement with observed ice water paths (Storelvmo et al., 2008). The method for determining cloud phase separation in Korolev and Mazin (2003) is described in Text S3 (Supporting Information S1).

Here we make highly idealized changes to explore the influence of cloud phase on the Miocene TS. Both Control and Modified simulations were run for 1854 years, and the last 50-year climatology was used in our analyses. Comparable simulations under modern "slab ocean" conditions yielded similar results, as reported by Dicks (2019). These simulations demonstrate that modified cloud microphysics leads to a stronger TS increase in the Arctic than in the tropics and reduces Arctic surface temperature seasonality. This consistency strengthens confidence that our findings are not artifacts due to a lack of equilibration or spurious effects of paleo-boundary conditions.

In the following sections, "differences" refer to those between the Modified and Control experiments (Modified-Control). "DJF" denotes boreal winter (December–January–February), and "JJA" denotes boreal summer (June–July–August).

3. Results

3.1. Differences in Global Mean Cloud Properties, Radiative Fluxes, and Surface Temperature

Imposed cloud microphysics changes lead to a 9.4% absolute increase in the annual global mean total cloud amount, with low-level, mid-level, and high-level clouds increasing by 1.1%, 0.8%, and 14.7% (Table S1 in Supporting Information S1), respectively. The annual global mean total grid-box cloud liquid water path (LWP) increases by 13.5% from 43.4 to 49.2 g/m^2, while the total grid-box cloud ice water path (IWP) increases by 150% from 15.4 to 39 g/m^2. The longwave cloud forcing (CF) increases by 15.7 W/m^2, offset by a shortwave CF change of −15.3 W/m^2, resulting in an insignificant change in total CF. Clear-sky radiative fluxes at surface or top of atmosphere show a slight relative change of −1.3%–0.5%, while all-sky radiative fluxes exhibit a relative decrease of 6%–9% (Table S1 in Supporting Information S1), indicating that cloud changes are the major contributor. There is no significant change in annual global mean top-of-atmosphere or surface energy budget residuals (Table S1 in Supporting Information S1), but the GMST increases by 1.5°C.

3.2. Differences in Zonal Mean Cloud Properties, Cloud Radiative Forcings, and Surface Temperatures

The most significant difference in cloud fraction between the Modified and Control experiments is an increase in annual zonal mean high-level cloud cover across all latitudes (Figures 2a and S1c in Supporting Information S1). The increase in mid-level cloud cover occurs primarily at high latitudes (Figure S1b in Supporting Information S1), while, in contrast, annual mean low-level cloud cover in high latitudes is reduced (Figure S1a in Supporting Information S1). Due to the significant increase in high-level cloud cover, total cloud cover increases across all latitudes (Figure 2d). In addition, both annual zonal mean cloud ice and liquid amounts increase across all latitudes (Figures 2b and 2c). The largest increase in cloud ice amount and grid-box cloud IWP is observed at high latitudes (60°-90°N/S) (Figures 2b and 2e), while the largest increase in grid-box cloud LWP occurs between 50° and 70°N/S (Figures 2c and 2f). The increase in cloud ice amount occurs in middle- and high-level clouds (Figure 2b), which are dominated by mixed-phase clouds that can form between −40°C and 0°C, as well as ice clouds. In contrast, the increase in cloud liquid mainly occurs in low-level clouds, including liquid clouds and the transition between liquid and mixed-phase clouds near the 0°C isotherm (Figure 2c).

Despite increases in both cloud ice and cloud liquid amounts across all latitudes, changes in the supercooled cloud fraction (SCF)—defined as the ratio of supercooled liquid to the total amount of supercooled liquid and ice within mixed-phase clouds, and used to quantify cloud water phase partitioning (Komurcu et al., 2014; Storelvmo et al., 2015)—are not uniform (Figure S2 in Supporting Information S1). The tropics exhibit an increase in SCF, whereas high latitudes experience a decrease (Figures S2j–S2l in Supporting Information S1). These changes primarily occur along isotherms between −5°C and −20°C, with minimal changes observed along isotherms below −20°C (Figures S2g–S2i in Supporting Information S1).

10.1029/2024GL111831

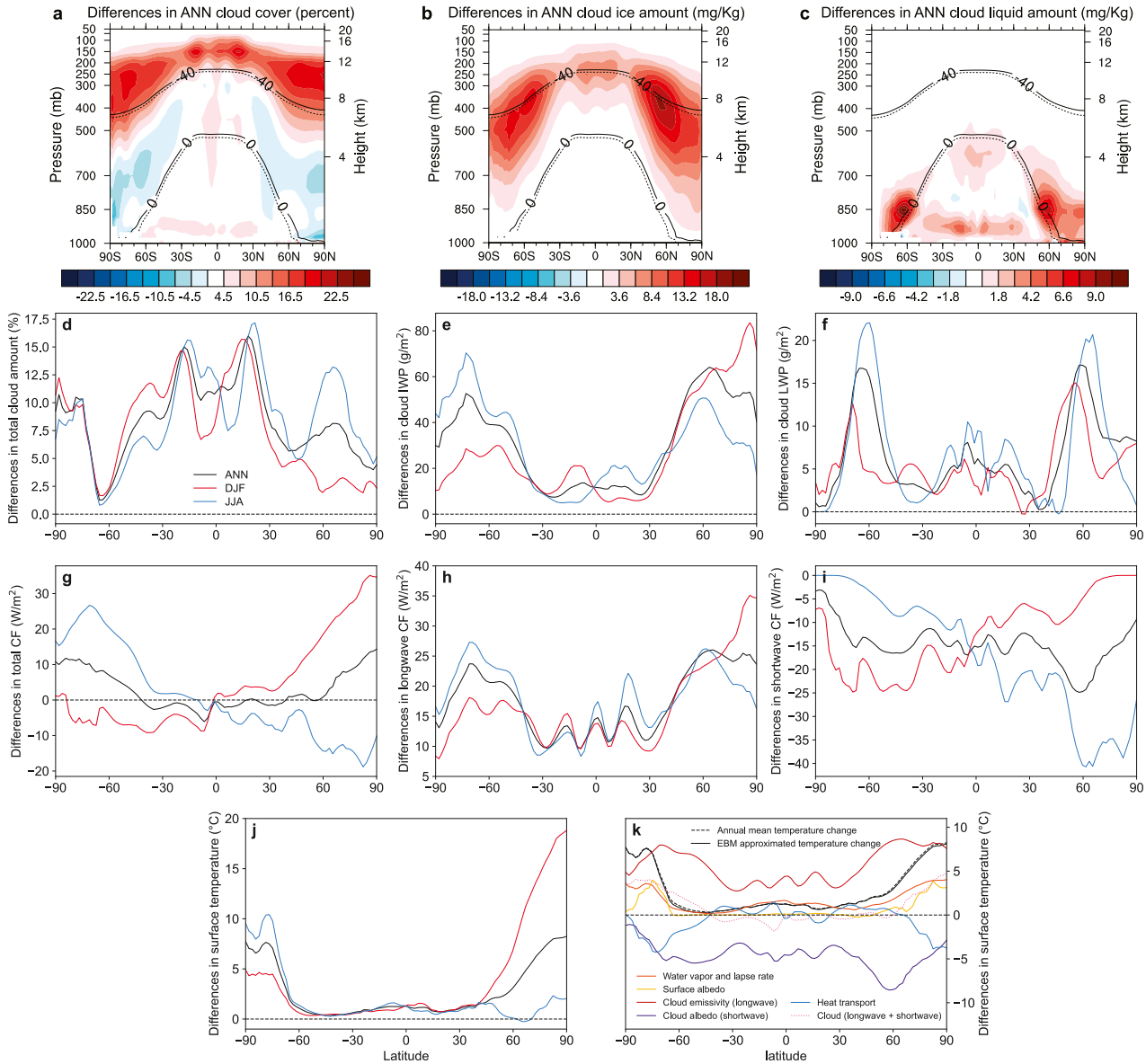

Figure 2. Zonal mean differences between the Modified and Control experiments in the vertical profile of annual mean cloud cover (a), cloud ice amount (b) and cloud liquid amount (c), total cloud amount (d), total grid-box cloud ice water path (e), total grid-box cloud liquid water path (f), total cloud forcing (g), longwave cloud forcing (h), shortwave cloud forcing (i), surface temperature (j), and surface temperature derived from a zonal-mean energy balance analysis (k). Dashed and solid lines in (a)–(c) indicate the isotherms of 0°C and −40°C in our Control and Modified experiments, respectively. Black, red, and blue lines in (d)–(j) represent the annual (ANN), DJF and JJA mean results, respectively. (k) shows the ANN mean results.

Changes in clouds and cloud properties increase the annual zonal mean longwave CF (LWCF) across all latitudes (Figure 2h), with the largest increase in northern high latitudes. This increase in annual mean LWCF (warming effect) is offset by an increase in shortwave CF (SWCF) (cooling effect) (Figure 2i). As a result, annual mean total CF shows a slight decrease of 1.7 W/m^2 averaged over tropical regions, with the largest increase in high latitudes (Figure 2g), showing increases of 8.8 W/m^2 and 10 W/m^2 in northern and southern regions, respectively. This indicates a net cooling effect in the tropics and a net warming effect in high latitudes due to total cloud forcing (Figure 2k), which reduces meridional temperature gradients.

The Modified experiment shows an increase in the annual zonal mean surface temperature (TS) across all latitudes compared to the Control experiment, with muted warming in the tropics and enhanced warming in high latitudes (Figure 2j), leading to reduced meridional surface temperature gradients. Polar warming is stronger in

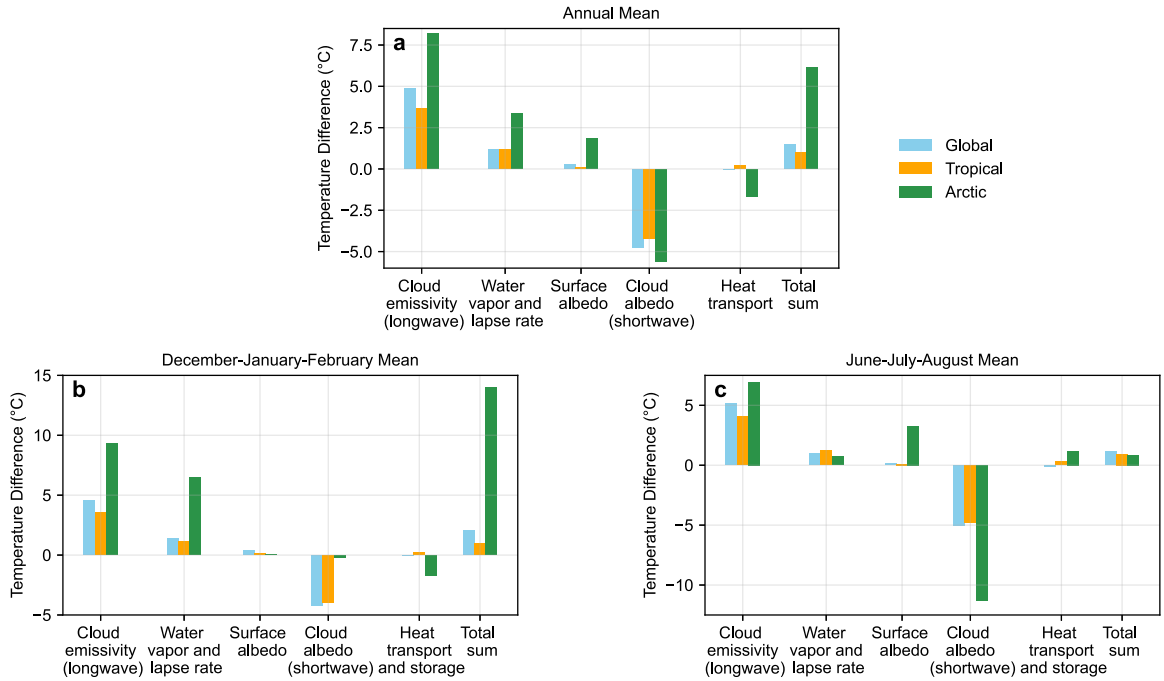

Figure 3. Global, tropical (30°S–30°N), and Arctic (67°N–90°N) mean surface temperature differences between the Modified and Control experiments, computed using a 1-D energy balance model framework.

DJF than in JJA, especially in the Arctic (67°N–90°N), with 14°C DJF warming and ∼1°C JJA warming (Figure 2j). The larger increase in Arctic mean TS during DJF compared to JJA (Figure 2j) reflects reduced seasonality, which is further supported by decreased annual TS ranges across all Arctic regions (Figure S3 in Supporting Information S1). This seasonality of Arctic warming, characterized by peak winter warming, is also a prominent feature of recent (Screen & Simmonds, 2010) and projected future climate change (Hahn et al., 2021; Holland & Bitz, 2003).

3.3. Mechanisms Causing Zonal Mean Surface Temperature Differences

To disentangle relative contributions of each radiative component and meridional heat transport to zonal mean TS changes, we conducted a one-dimensional energy balance analysis (Text S4, Figures 2k and S4 in Supporting Information S1), using the framework formulated by Heinemann et al. (2009) and Lunt et al. (2012). The analysis suggests that increased LWCF due to changes in cloud emissivity is a primary driver of annual zonal mean TS increases (Figure 2k). In the tropics, the annual mean warming due to LWCF (3.69°C) is offset by cooling from SWCF due to changes in cloud albedo (−4.2°C) (Figure 3a), resulting in a net cooling that aligns with the decreased total cloud forcing (Figure 1a). Despite this net cooling, muted warming is observed in the tropics (Figure 2j), driven by reduced poleward atmospheric heat transport and amplified by a positive water vapor feedback (Figures 2k and 3a). In the Arctic, the annual mean warming due to LWCF (8.19°C) surpasses the cooling from SWCF (−5.58°C) (Figure 3a), generating a net warming (Figure 2j). The secondary contribution to the Arctic annual mean TS increase comes from changes in water vapor and lapse rate (Figures 2k and 3a). The Arctic warming (1.86°C) driven by the positive surface albedo feedback is almost canceled out by the cooling (−1.64°C) from reduced meridional heat transport, which is likely caused by the reduced meridional temperature gradients.

The pattern, where LWCF plays a primary role and water vapor and lapse rate serve as secondary drivers of the Arctic annual mean TS increase, is mainly observed in DJF (Figures 3b and S4a in Supporting Information S1): LWCF contributes to 9.31°C of warming, while water vapor and lapse rate add 3.33°C, and SWCF causes a slight cooling of 0.18°C. In contrast, during JJA, surface albedo changes become the secondary driver in Arctic warming, with minimal contributions from water vapor and lapse rate (Figures 3c and S4b in Supporting Information S1). Compared to JJA, the larger Arctic TS increase in DJF is due to a greater warming effect from

changes in LWCF, water vapor, and lapse rate, as well as a weaker cooling effect from changes in SWCF (Figures 3b and 3c). This is reflected in two key features of changes in the annual cycle of Arctic longwave and shortwave fluxes. First, the largest increase occurs in DJF for LWCF at the top of the atmosphere (Figure S5a in Supporting Information S1) and surface (Figure S5c in Supporting Information S1), as well as for clear-sky surface downwelling longwave flux (Figure S5f in Supporting Information S1) associated with water vapor and lapse rate. Second, the largest increase occurs in JJA for SWCF at the top of the atmosphere (Figure S5b in Supporting Information S1) and surface (Figure S5d in Supporting Information S1).

Additionally, calculations of atmospheric radiative flux changes due to various feedbacks (Janoski et al., 2024) using the radiative kernel for CAM5 (Pendergrass et al., 2018) confirm that longwave cloud feedback is the primary driver of the TS increase across all latitudes (Figure S6 in Supporting Information S1), particularly in the Arctic. Consistent with the 1-D energy balance analysis, these calculations also show that the second-largest contributor to the Arctic TS increase is water vapor and lapse rate feedback in winter and surface albedo feedback in summer (Figures S6 and S7 in Supporting Information S1). However, it is important to note that these calculations may be biased, as the radiative kernel depends on the base climate and is typically derived using the modern climate as a reference (Soden et al., 2008). Since feedback strengths (e.g., water vapor, lapse rate, and cloud feedback) can vary with climate state (Colman & Soden, 2021; Zhu & Poulsen, 2020), a radiative kernel based on modern climate may not be fully applicable to paleoclimate studies.

4. Discussion

4.1. Influences of Cloud Properties on Longwave Cloud Forcing

As explained in Sections 3.2 and 3.3, the zonal-mean TS increase, especially in the Arctic, is primarily attributed to the increase in LWCF. This LWCF increase likely results from increases in cloud ice water content (Figures 2b and 2e) and cloud cover (Figure 2a).

Since cloud optical depth depends on cloud water content and particle size, clouds with higher ice water content have greater optical depth, leading to stronger longwave cloud radiative effects (Hong & Liu, 2015). The increased zonal-mean LWCF between our Modified and Control experiments (Figure 2h) likely results from higher cloud ice water content (Figures 2b and 2e), which is supported by the fact that differences in zonal-mean LWCF (Figure 2h) correlate well with those in IWP (Figure 2e), with correlation coefficients of 0.95, 0.96, and 0.87 for the annual, DJF, and JJA means, respectively. An increase in LWP also contributes to the enhanced LWCF, particularly during the Arctic winter. Cloud emissivity and LWCF are more sensitive to changes in LWP when it is below 30 g/m^2 (Shupe & Intrieri, 2004; Stephens, 1978), a condition more prevalent in high latitudes than in the tropics and mid-latitudes (Figure S8 in Supporting Information S1). This sensitivity is especially pronounced during the Arctic winter (DJF), where LWP increases from 0.78 to 5.85 g/m^2, compared to annual mean increases from 17.89 to 26.95 g/m^2 and summer (JJA) increases from 49.52 to 60.05 g/m^2 (Figure S8 in Supporting Information S1).

Additionally, considering the warming effect of high-level ice clouds (Gasparini & Lohmann, 2016; Hong et al., 2016; Khvorostyanov & Sassen, 2002; Lohmann & Gasparini, 2017), the significant increase in high-level ice cloud fractions across all latitudes in the Modified experiment (Figures 2a and S1c in Supporting Information S1) contributes to increased LWCF, which is reflected in a reduced longwave cooling rate in the upper troposphere with ice clouds (Figure S9 in Supporting Information S1). Although both ice and liquid water contents increase, the dominance of ice cloud effects renders changes in mixed-phase clouds, SCF, and their influences relatively less significant.

These differences in Arctic cloud and cloud properties result from the modifications in ice nucleation and cloud phase partitioning schemes. The modified aerosol-dependent ice nucleation scheme from DeMott et al. (2015) tends to reduce the IN concentrations and ice crystal number concentrations, decrease IWP, and increase LWP in high latitudes, due to the slowdown of the WBF process in mixed-phase clouds, as shown in previous studies by Xie et al. (2013) and Komurcu et al. (2014) using a similar scheme from DeMott et al. (2010). The implementation of the theory-based cloud phase partitioning framework from Korolev and Mazin (2003) tends to increase the ice crystal number concentrations, increase the IWP, and decrease the LWP, as suggested by Storelvmo et al. (2008). This occurs due to a new treatment of the WBF processes, where glaciation begins as soon as any ice forms, even in tiny amounts (Storelvmo et al., 2008). In contrast, the treatment in the Control experiment allows clouds to

remain predominantly liquid at very low temperatures, provided the critical ice mixing ratio required to initiate the WBF process is not reached. Together, these two modifications cause a net increase in LWP, IWP, and mid- and high-level clouds in our Modified experiment. The interactions between ice nucleation, growth, and cloud phase are complex, and further experiments are needed to determine their individual effects on the obtained warming.

Despite this complexity, the increase in cloud ice likely results from higher water vapor content and a more efficient WBF process in the Modified experiment. The greater cloud ice content in ice clouds (Figure 2b), along with higher ice number concentrations (Figures S10a–S10c in Supporting Information S1) and larger ice effective radius (Figures S10d–S10f in Supporting Information S1), is likely driven by increased water vapor content (Figures S10g–S10i in Supporting Information S1) available for ice crystal growth. In mixed-phase clouds, higher water vapor content and a more efficient WBF process contribute to the increase in cloud ice. The enhanced WBF efficiency is evidenced by larger ice effective radii in mixed-phase clouds between the 0°C and −20°C isotherms (Figures S10d–S10f in Supporting Information S1), where the SCF changes significantly (Figures S2g–S2i in Supporting Information S1). A stronger WBF process likely also occurs between the −20°C and −40°C isotherms, increasing ice number concentrations (Figures S10a–S10c in Supporting Information S1) through rapid freezing of liquid droplets and reducing ice effective radii (Figures S10d–S10f in Supporting Information S1) due to the limited water vapor content being distributed among numerous ice crystals.

4.2. Contributions From Changes in Water Vapor and Lapse Rate

Besides increased LWCF, the larger TS increase in the Arctic compared to the tropics, especially in DJF, is also attributed to changes in water vapor and lapse rate (Figures 2k and S4a in Supporting Information S1). In the Modified experiment, the relative increase in specific humidity (Figure S11b in Supporting Information S1) during DJF in the near-surface troposphere coincides with the temperature rise (Figure S11a in Supporting Information S1), with both showing greater increases in the Arctic than in the tropics. The stronger Arctic warming driven by LWCF leads to a greater relative increase in water vapor content (Figure S11b in Supporting Information S1), which could potentially cause more warming (Graversen & Wang, 2009), as water vapor is an efficient greenhouse gas. However, decomposition of changes in atmospheric radiative fluxes using the radiative kernel suggests that water vapor feedback is weak whereas lapse rate feedback is relatively strong in the Arctic winter (Figures S6 and S7 in Supporting Information S1).

The positive lapse rate feedback in the Arctic winter, related to a stably stratified inversion layer that hampers vertical mixing (Boeke et al., 2021; Feldl et al., 2020), has been identified as a key driver of Arctic amplification (Bintanja et al., 2011; Linke et al., 2023; Pithan & Mauritsen, 2014). Compared with the Control experiment, the Modified experiment shows a weaker Arctic winter temperature inversion (Figure S12 in Supporting Information S1) and lower-tropospheric stability—calculated as the difference in potential temperature between the free troposphere (700 hPa) and the surface (Figure S13 in Supporting Information S1). These changes indicate that a positive lapse rate feedback between the Control and Modified experiments amplifies surface warming.

4.3. Low Gradient and Equable Climate Problem

The modifications made in our simulations increase the GMST by 1.6°C, from 18.6°C (Control) to 20.2°C (Modified), bringing it closer to the lower end of proxy-derived Mid-Miocene estimates (21.21 ± 0.56°C) (Burls et al., 2021a). Our modifications also reduce the equator-to-pole temperature difference from 35.44°C to 31.56°C (Table S2 in Supporting Information S1), although still above proxy-based values (12.42 ± 2.78°C) with this discrepancy primarily arising from high-latitude estimates (Table S2 in Supporting Information S1), and decrease high-latitude continental TS seasonality (Figure S3 in Supporting Information S1). These are two common features of past greenhouse climates that are difficult to replicate with climate models (Huber, 2013), known as low gradient and equable continental climate problems. Our study suggests that a more realistic representation of processes affecting cloud phase, compared to the default parameterizations in CAM5.1, can help mitigate these problems. This is consistent with the fact that more recent versions of CAM, which include related microphysical improvements, also reproduce past warm climates better (Feng et al., 2020; Zhu et al., 2019).

5. Conclusions and Implications

Our results demonstrate that modeled surface temperatures of the early-to-middle Miocene are sensitive to changes in parameterizations of processes affecting cloud phase. Modifying the frameworks of ice nucleation and ice crystal growth, both of which influence cloud phase, in Miocene climate modeling increases mid- and high-level cloud amounts and cloud water content across all latitudes. These changes enhance both zonal-mean LWCF and SWCF, resulting in a slight decrease in annual zonal mean total CF in the tropics and significant increases at high latitudes, including the Arctic. The modification leads to an increase in GMST, with a smaller TS increase in the tropics and the most pronounced TS increase in the Arctic, particularly during winter. Consequently, this results in a reduced meridional surface temperature gradient and decreased seasonality of the Arctic TS. The annual mean Arctic TS increase is primarily driven by increased LWCF, with secondary contributions from water vapor and lapse rate changes. This pattern is most pronounced in Arctic winter. In contrast, during Arctic summer, surface albedo changes become the second-largest contributor, while the contributions from water vapor and lapse rate changes are minimal. These findings suggest that improving the representation of processes affecting cloud phase, specifically ice nucleation and the WBF process, in models may improve their ability to simulate the high-latitude warmth of the early-to-middle Miocene. Our study highlights sensitivities of polar amplification and climate sensitivity to plausible changes in cloud microphysics, and specifically in this case underscores the importance of processes influencing cloud phase and longwave radiative forcing.

Data Availability Statement

NCAR CESM1.0 is an open-source community model, and is available at: https://www2.cesm.ucar.edu/models/cesm1.0/. The Miocene boundary conditions used in the simulations are publicly available at Burls et al. (2021b). Model outputs and modified source code used in this study are available at Liu et al. (2024). The Python package for calculating radiative feedbacks using radiative kernels is developed by Janoski et al. (2024) and available at https://github.com/tyfolino/climkern/.

Acknowledgments
The CESM project is supported primarily by the National Science Foundation. We are grateful to the National Science Foundation Grant (#1602905 and #2217530) and Institute for a Sustainable Future at Purdue University for funding our study. M. Komurcu would like to extend gratitude to Daniel J. Cziczo, Chien Wang and David McGee of MIT for providing material resources to complete part of the work. We acknowledge the Rosen Center for Advanced Computing at Purdue University for providing computational support. We would like to thank the Editor for handling the review process of this manuscript and the three anonymous reviewers for their constructive feedback and insightful comments that have improved this work.

References

Abbot, D. S., & Tziperman, E. (2008a). A high-latitude convective cloud feedback and equable climates. *Quarterly Journal of the Royal Meteorological Society*, *134*(630), 165–185. https://doi.org/10.1002/qj.211

Abbot, D. S., & Tziperman, E. (2008b). Sea ice, high-latitude convection, and equable climates. *Geophysical Research Letters*, *35*(3). https://doi.org/10.1029/2007GL032286

Barron, E. J., Fawcett, P. J., Peterson, W. H., Pollard, D., & Thompson, S. L. (1995). A "simulation" of Mid-Cretaceous climate. *Paleoceanography*, *10*(5), 953–962. https://doi.org/10.1029/95PA01624

Bintanja, R., Graversen, R. G., & Hazeleger, W. (2011). Arctic winter warming amplified by the thermal inversion and consequent low infrared cooling to space. *Nature Geoscience*, *4*(11), 758–761. https://doi.org/10.1038/ngeo1285

Boeke, R. C., Taylor, P. C., & Sejas, S. A. (2021). On the nature of the Arctic's positive lapse-rate feedback. *Geophysical Research Letters*, *48*(1), e2020GL091109. https://doi.org/10.1029/2020GL091109

Burls, N. J., Bradshaw, C. D., De Boer, A. M., Herold, N., Huber, M., Pound, M., et al. (2021a). Simulating miocene warmth: Insights from an opportunistic multi-model ensemble (MioMIP1). *Paleoceanography and Paleoclimatology*, *36*(5), e2020PA004054. https://doi.org/10.1029/2020PA004054

Burls, N. J., Bradshaw, C. D., De Boer, A. M., Herold, N., Huber, M., Pound, M., et al. (2021b). Simulating miocene warmth: Insights from an opportunistic multi-model ensemble (MioMIP1). *Zenodo*, *36*(5). [Dataset]. https://doi.org/10.5281/zenodo.4568897

Burls, N. J., & Fedorov, A. V. (2014). Simulating Pliocene warmth and a permanent El Niño-like state: The role of cloud albedo. *Paleoceanography*, *29*(10), 893–910. https://doi.org/10.1002/2014PA002644

Cesana, G., Waliser, D. E., Jiang, X., & Li, J.-L. F. (2015). Multimodel evaluation of cloud phase transition using satellite and reanalysis data. *Journal of Geophysical Research: Atmospheres*, *120*(15), 7871–7892. https://doi.org/10.1002/2014JD022932

Colman, R., & Soden, B. J. (2021). Water vapor and lapse rate feedbacks in the climate system. *Reviews of Modern Physics*, *93*(4), 045002. https://doi.org/10.1103/RevModPhys.93.045002

DeMott, P. J., Prenni, A. J., Liu, X., Kreidenweis, S. M., Petters, M. D., Twohy, C. H., et al. (2010). Predicting global atmospheric ice nuclei distributions and their impacts on climate. *Proceedings of the National Academy of Sciences*, *107*(25), 11217–11222. https://doi.org/10.1073/pnas.0910818107

DeMott, P. J., Prenni, A. J., McMeeking, G. R., Sullivan, R. C., Petters, M. D., Tobo, Y., et al. (2015). Integrating laboratory and field data to quantify the immersion freezing ice nucleation activity of mineral dust particles. *Atmospheric Chemistry and Physics*, *15*(1), 393–409. https://doi.org/10.5194/acp-15-393-2015

Dicks, A. J. (2019). *Understanding Miocene climatic warmth (Master's Thesis)*. Purdue University. https://doi.org/10.25394/PGS.8956736.v1

Dutta, D., Jucker, M., Sherwood, S. C., Meissner, K. J., Sen Gupta, A., & Zhu, J. (2023). Early Eocene low orography and high methane enhance Arctic warming via polar stratospheric clouds. *Nature Geoscience*, *16*(11), 1027–1032. https://doi.org/10.1038/s41561-023-01298-w

Dutta, D., Sherwood, S. C., Jucker, M., Gupta, A. S., & Meissner, K. J. (2023). Can polar stratospheric clouds explain arctic amplification? *Journal of Climate*, *36*(8), 2313–2332. https://doi.org/10.1175/JCLI-D-22-0497.1

Evans, D., Brugger, J., Inglis, G. N., & Valdes, P. (2024). The temperature of the deep ocean is a robust proxy for global mean surface temperature during the Cenozoic. *Paleoceanography and Paleoclimatology*, *39*(5), e2023PA004788. https://doi.org/10.1029/2023PA004788

Feldl, N., Po-Chedley, S., Singh, H. K. A., Hay, S., & Kushner, P. J. (2020). Sea ice and atmospheric circulation shape the high-latitude lapse rate feedback. *npj Climate and Atmospheric Science*, *3*(1), 41. https://doi.org/10.1038/s41612-020-00146-7

Feng, R., Otto-Bliesner, B. L., Brady, E. C., & Rosenbloom, N. (2020). Increased climate response and Earth system sensitivity from CCSM4 to CESM2 in mid-pliocene simulations. *Journal of Advances in Modeling Earth Systems*, *12*(8), e2019MS002033. https://doi.org/10.1029/2019MS002033

Feng, R., Otto-Bliesner, B. L., Xu, Y., Brady, E., Fletcher, T., & Ballantyne, A. (2019). Contributions of aerosol-cloud interactions to mid-Piacenzian seasonally sea ice-free Arctic Ocean. *Geophysical Research Letters*, *46*(16), 9920–9929. https://doi.org/10.1029/2019GL083960

Frazer, M. E., & Ming, Y. (2022). Understanding the extratropical liquid water path feedback in mixed-phase clouds with an idealized global climate model. *Journal of Climate*, *35*(8), 2391–2406. https://doi.org/10.1175/JCLI-D-21-0334.1

Frey, W. R., & Kay, J. E. (2018). The influence of extratropical cloud phase and amount feedbacks on climate sensitivity. *Climate Dynamics*, *50*(7), 3097–3116. https://doi.org/10.1007/s00382-017-3796-5

Gasparini, B., & Lohmann, U. (2016). Why cirrus cloud seeding cannot substantially cool the planet. *Journal of Geophysical Research: Atmospheres*, *121*(9), 4877–4893. https://doi.org/10.1002/2015JD024666

Goldner, A., Herold, N., & Huber, M. (2014). The challenge of simulating the warmth of the mid-Miocene climatic optimum in CESM1. *Climate of the Past*, *10*(2), 523–536. https://doi.org/10.5194/cp-10-523-2014

Graversen, R. G., & Wang, M. (2009). Polar amplification in a coupled climate model with locked albedo. *Climate Dynamics*, *33*(5), 629–643. https://doi.org/10.1007/s00382-009-0535-6

Hahn, L. C., Armour, K. C., Zelinka, M. D., Bitz, C. M., & Donohoe, A. (2021). Contributions to polar amplification in CMIP5 and CMIP6 models. *Frontiers in Earth Science*, *9*. https://doi.org/10.3389/feart.2021.710036

Hay, W. W., DeConto, R. M., de Boer, P., Flögel, S., Song, Y., & Stepashko, A. (2019). Possible solutions to several enigmas of Cretaceous climate. *International Journal of Earth Sciences*, *108*(2), 587–620. https://doi.org/10.1007/s00531-018-1670-2

Hay, W. W., DeConto, R. M., & Wold, C. N. (1997). Climate: Is the past the key to the future? *Geologische Rundschau*, *86*(2), 471–491. https://doi.org/10.1007/s005310050155

Haywood, A. M., Dowsett, H. J., & Dolan, A. M. (2016). Integrating geological archives and climate models for the mid-Pliocene warm period. *Nature Communications*, *7*(1), 10646. https://doi.org/10.1038/ncomms10646

Haywood, A. M., Tindall, J. C., Dowsett, H. J., Dolan, A. M., Foley, K. M., Hunter, S. J., et al. (2020). The Pliocene model intercomparison project phase 2: Large-scale climate features and climate sensitivity. *Climate of the Past*, *16*(6), 2095–2123. https://doi.org/10.5194/cp-16-2095-2020

Heinemann, M., Jungclaus, J. H., & Marotzke, J. (2009). Warm paleocene/eocene climate as simulated in ECHAM5/MPI-OM. *Climate of the Past*, *5*(4), 785–802. https://doi.org/10.5194/cp-5-785-2009

Herold, N., Huber, M., & Müller, R. D. (2011). Modeling the miocene climatic optimum. Part I: Land and atmosphere. *Journal of Climate*, *24*(24), 6353–6372. https://doi.org/10.1175/2011JCLI4035.1

Holbourn, A., Kuhnt, W., Regenberg, M., Schulz, M., Mix, A., & Andersen, N. (2010). Does Antarctic glaciation force migration of the tropical rain belt? *Geology*, *38*(9), 783–786. https://doi.org/10.1130/G31043.1

Holland, M. M., & Bitz, C. M. (2003). Polar amplification of climate change in coupled models. *Climate Dynamics*, *21*(3–4), 221–232. https://doi.org/10.1007/s00382-003-0332-6

Hong, Y., & Liu, G. (2015). The characteristics of ice cloud properties derived from CloudSat and CALIPSO measurements. *Journal of Climate*, *28*(9), 3880–3901. https://doi.org/10.1175/JCLI-D-14-00666.1

Hong, Y., Liu, G., & Li, J.-L. F. (2016). Assessing the radiative effects of global ice clouds based on CloudSat and CALIPSO measurements. *Journal of Climate*, *29*(21), 7651–7674. https://doi.org/10.1175/JCLI-D-15-0799.1

Huber, M. (2012). Progress in greenhouse climate modeling. *Paleontological Society Papers*, *18*, 213–262. https://doi.org/10.1017/S108933260000262X

Huber, M. (2013). A sensitivity to history. *Nature Geoscience*, *6*(1), 15–16. https://doi.org/10.1038/ngeo1695

Janoski, T. P., Mitevski, I., & Wen, K. (2024). *Climkern*. Zenodo. https://doi.org/10.5281/zenodo.10291284

Khvorostyanov, V. I., & Sassen, K. (2002). Microphysical processes in cirrus and their impact on radiation: A mesoscale modeling perspective. In D. K. Lynch, K. Sassen, D. O. Starr, & G. Stephens (Eds.), *Cirrus* (p. 0). Oxford University Press. https://doi.org/10.1093/oso/9780195130720.003.0023

Kirk-Davidoff, D. B., Schrag, D. P., & Anderson, J. G. (2002). On the feedback of stratospheric clouds on polar climate. *Geophysical Research Letters*, *29*(11), 51–61. https://doi.org/10.1029/2002GL014659

Komurcu, M., Storelvmo, T., Tan, I., Lohmann, U., Yun, Y., Penner, J. E., et al. (2014). Intercomparison of the cloud water phase among global climate models. *Journal of Geophysical Research: Atmospheres*, *119*(6), 3372–3400. https://doi.org/10.1002/2013JD021119

Korolev, A. V., & Mazin, I. P. (2003). Supersaturation of water vapor in clouds. *Journal of the Atmospheric Sciences*, *60*(24), 2957–2974. https://doi.org/10.1175/1520-0469(2003)060⟨2957:SOWVIC⟩2.0.CO;2

Kump, L. R., & Pollard, D. (2008). Amplification of cretaceous warmth by biological cloud feedbacks. *Science*, *320*(5873), 195. https://doi.org/10.1126/science.1153883

Li, G., Pettke, T., & Chen, J. (2011). Increasing Nd isotopic ratio of Asian dust indicates progressive uplift of the north Tibetan Plateau since the middle Miocene. *Geology*, *39*(3), 199–202. https://doi.org/10.1130/G31734.1

Li, Z.-X., & Le Treut, H. (1992). Cloud-radiation feedbacks in a general circulation model and their dependence on cloud modelling assumptions. *Climate Dynamics*, *7*(3), 133–139. https://doi.org/10.1007/BF00211155

Linke, O., Quaas, J., Baumer, F., Becker, S., Chylik, J., Dahlke, S., et al. (2023). Constraints on simulated past Arctic amplification and lapse rate feedback from observations. *Atmospheric Chemistry and Physics*, *23*(17), 9963–9992. https://doi.org/10.5194/acp-23-9963-2023

Liu, X., Easter, R. C., Ghan, S. J., Zaveri, R., Rasch, P., Shi, X., et al. (2012). Toward a minimal representation of aerosols in climate models: Description and evaluation in the Community Atmosphere Model CAM5. *Geoscientific Model Development*, *5*(3), 709–739. https://doi.org/10.5194/gmd-5-709-2012

Liu, X., Griffin, A., Komurcu, M., & Huber, M. (2024). Importance of longwave radiative forcing by icy clouds in maintaining miocene high-latitude warmth. *Zenodo*. [Dataset]. https://doi.org/10.5281/zenodo.13984465

Lohmann, U., & Gasparini, B. (2017). A cirrus cloud climate dial? *Science*, *357*(6348), 248–249. https://doi.org/10.1126/science.aan3325

Lunt, D. J., Bragg, F., Chan, W.-L., Hutchinson, D. K., Ladant, J.-B., Morozova, P., et al. (2021). DeepMIP: Model intercomparison of early Eocene climatic optimum (EECO) large-scale climate features and comparison with proxy data. *Climate of the Past*, *17*(1), 203–227. https://doi.org/10.5194/cp-17-203-2021

Lunt, D. J., Dunkley Jones, T., Heinemann, M., Huber, M., LeGrande, A., Winguth, A., et al. (2012). A model–data comparison for a multi-model ensemble of early eocene atmosphere–ocean simulations: EoMIP. *Climate of the Past*, *8*(5), 1717–1736. https://doi.org/10.5194/cp-8-1717-2012

McCoy, D. T., Field, P., Frazer, M. E., Zelinka, M. D., Elsaesser, G. S., Mülmenstädt, J., et al. (2022). Extratropical shortwave cloud feedbacks in the context of the global circulation and hydrological cycle. *Geophysical Research Letters*, *49*(8), e2021GL097154. https://doi.org/10.1029/2021GL097154

Meyers, M. P., DeMott, P. J., & Cotton, W. R. (1992). New primary ice-nucleation parameterizations in an explicit cloud model. *Journal of Applied Meteorology and Climatology*, *31*(7), 708–721. https://doi.org/10.1175/1520-0450(1992)031⟨0708:NPINPI⟩2.0.CO;2

Mitchell, J. F. B., Senior, C. A., & Ingram, W. J. (1989). C02 and climate: A missing feedback? *Nature*, *341*(6238), 132–134. https://doi.org/10.1038/341132a0

Morrison, H., & Gettelman, A. (2008). A new two-moment bulk stratiform cloud microphysics scheme in the community atmosphere model, version 3 (CAM3). Part I: Description and numerical tests. *Journal of Climate*, *21*(15), 3642–3659. https://doi.org/10.1175/2008JCLI2105.1

Niezgodzki, I., Knorr, G., Lohmann, G., Tyszka, J., & Markwick, P. J. (2017). Late cretaceous climate simulations with different CO2 levels and subarctic gateway configurations: A model-data comparison. *Paleoceanography*, *32*(9), 980–998. https://doi.org/10.1002/2016PA003055

O'Brien, C. L., Huber, M., Thomas, E., Pagani, M., Super, J. R., Elder, L. E., & Hull, P. M. (2020). The enigma of Oligocene climate and global surface temperature evolution. *Proceedings of the National Academy of Sciences*, *117*(41), 25302–25309. https://doi.org/10.1073/pnas.2003914117

Pagani, M., Huber, M., & Sageman, B. (2014). 6.13 – greenhouse climates. In H. D. Holland & K. K. Turekian (Eds.), *Treatise on geochemistry* (2nd ed., pp. 281–304). Elsevier. https://doi.org/10.1016/B978-0-08-095975-7.01314-0

Pendergrass, A. G., Conley, A., & Vitt, F. M. (2018). Surface and top-of-atmosphere radiative feedback kernels for CESM-CAM5. *Earth System Science Data*, *10*(1), 317–324. https://doi.org/10.5194/essd-10-317-2018

Pithan, F., & Mauritsen, T. (2014). Arctic amplification dominated by temperature feedbacks in contemporary climate models. *Nature Geoscience*, *7*(3), 181–184. https://doi.org/10.1038/ngeo2071

Prenni, A. J., Harrington, J. Y., Tjernström, M., DeMott, P. J., Avramov, A., Long, C. N., et al. (2007). Can ice-nucleating aerosols affect arctic seasonal climate? *Bulletin of the American Meteorological Society*, *88*(4), 541–550. https://doi.org/10.1175/BAMS-88-4-541

Rae, J. W., Zhang, Y. G., Liu, X., Foster, G. L., Stoll, H. M., & Whiteford, R. D. (2021). Atmospheric CO2 over the past 66 million years from marine archives. *Annual Review of Earth and Planetary Sciences*, *49*(1), 609–641. https://doi.org/10.1146/annurev-earth-082420-063026

Sagoo, N., & Storelvmo, T. (2017). Testing the sensitivity of past climates to the indirect effects of dust. *Geophysical Research Letters*, *44*(11), 5807–5817. https://doi.org/10.1002/2017GL072584

Sagoo, N., Storelvmo, T., Hahn, L., Tan, I., Danco, J., Raney, B., & Broccoli, A. J. (2021). Observationally constrained cloud phase unmasks orbitally driven climate feedbacks. *Geophysical Research Letters*, *48*(6), e2020GL091873. https://doi.org/10.1029/2020GL091873

Screen, J. A., & Simmonds, I. (2010). Increasing fall-winter energy loss from the Arctic Ocean and its role in Arctic temperature amplification. *Geophysical Research Letters*, *37*(16). https://doi.org/10.1029/2010GL044136

Shevenell, A. E., Kennett, J. P., & Lea, D. W. (2004). Middle miocene southern ocean cooling and Antarctic cryosphere expansion. *Science*, *305*(5691), 1766–1770. https://doi.org/10.1126/science.1100061

Shupe, M. D. (2011). Clouds at arctic atmospheric observatories. Part II: Thermodynamic phase characteristics. *Journal of Applied Meteorology and Climatology*, *50*(3), 645–661. https://doi.org/10.1175/2010JAMC2468.1

Shupe, M. D., & Intrieri, J. M. (2004). Cloud radiative forcing of the arctic surface: The influence of cloud properties, surface albedo, and solar zenith angle. *Journal of Climate*, *17*(3), 616–628. https://doi.org/10.1175/1520-0442(2004)017⟨0616:CRFOTA⟩2.0.CO;2

Sloan, L. C., & Pollard, D. (1998). Polar stratospheric clouds: A high latitude warming mechanism in an ancient greenhouse world. *Geophysical Research Letters*, *25*(18), 3517–3520. https://doi.org/10.1029/98GL02492

Soden, B. J., Held, I. M., Colman, R., Shell, K. M., Kiehl, J. T., & Shields, C. A. (2008). Quantifying climate feedbacks using radiative kernels. *Journal of Climate*, *21*(14), 3504–3520. https://doi.org/10.1175/2007JCLI2110.1

Sosdian, S. M., Greenop, R., Hain, M. P., Foster, G. L., Pearson, P. N., & Lear, C. H. (2018). Constraining the evolution of Neogene ocean carbonate chemistry using the boron isotope pH proxy. *Earth and Planetary Science Letters*, *498*, 362–376. https://doi.org/10.1016/j.epsl.2018.06.017

Sosdian, S. M., & Lear, C. H. (2020). Initiation of the Western Pacific warm pool at the middle miocene climate transition? *Paleoceanography and Paleoclimatology*, *35*(12), e2020PA003920. https://doi.org/10.1029/2020PA003920

Steinthorsdottir, M., Coxall, H. K., de Boer, A. M., Huber, M., Barbolini, N., Bradshaw, C. D., et al. (2021). The miocene: The future of the past. *Paleoceanography and Paleoclimatology*, *36*(4), e2020PA004037. https://doi.org/10.1029/2020PA004037

Steinthorsdottir, M., Jardine, P. E., & Rember, W. C. (2021). Near-future pCO2 during the hot miocene climatic optimum. *Paleoceanography and Paleoclimatology*, *36*(1), e2020PA003900. https://doi.org/10.1029/2020PA003900

Stephens, G. L. (1978). Radiation profiles in extended water clouds. II: Parameterization schemes. *Journal of the Atmospheric Sciences*, *35*(11), 2123–2132. https://doi.org/10.1175/1520-0469(1978)035⟨2123:RPIEWC⟩2.0.CO;2

Storelvmo, T., Kristjánsson, J. E., Lohmann, U., Iversen, T., Kirkevåg, A., & Seland, Ø. (2008). Modeling of the Wegener–Bergeron–Findeisen process—Implications for aerosol indirect effects. *Environmental Research Letters*, *3*(4), 045001. https://doi.org/10.1088/1748-9326/3/4/045001

Storelvmo, T., Tan, I., & Korolev, A. V. (2015). Cloud phase changes induced by CO2 warming—A powerful yet poorly constrained cloud-climate feedback. *Current Climate Change Reports*, *1*(4), 288–296. https://doi.org/10.1007/s40641-015-0026-2

Super, J. R., Thomas, E., Pagani, M., Huber, M., O'Brien, C. L., & Hull, P. M. (2020). Miocene evolution of north Atlantic sea surface temperature. *Paleoceanography and Paleoclimatology*, *35*(5), e2019PA003748. https://doi.org/10.1029/2019PA003748

Tan, I., Barahona, D., & Coopman, Q. (2022). Potential link between ice nucleation and climate model spread in arctic amplification. *Geophysical Research Letters*, *49*(4), e2021GL097373. https://doi.org/10.1029/2021GL097373

Tan, I., & Storelvmo, T. (2016). Sensitivity study on the influence of cloud microphysical parameters on mixed-phase cloud thermodynamic phase partitioning in CAM5. *Journal of the Atmospheric Sciences*, *73*(2), 709–728. https://doi.org/10.1175/JAS-D-15-0152.1

Tan, I., Storelvmo, T., & Zelinka, M. D. (2016). Observational constraints on mixed-phase clouds imply higher climate sensitivity. *Science*, *352*(6282), 224–227. https://doi.org/10.1126/science.aad5300

The Cenozoic CO2 Proxy Integration Project (CenCO2PIP) Consortium†, Hönisch, B., Royer, D. L., Breecker, D. O., Polissar, P. J., Bowen, G. J., et al. (2023). Toward a Cenozoic history of atmospheric CO2. *Science*, *382*(6675), eadi5177. https://doi.org/10.1126/science.adi5177

Wubben, E., Spiering, B. R., Veenstra, T., Bos, R., Wang, Z., van Dijk, J., et al. (2024). Tropical warming and intensification of the west African Monsoon during the miocene climatic optimum. *Paleoceanography and Paleoclimatology*, *39*(5), e2023PA004767. https://doi.org/10.1029/2023PA004767

Xie, S., Liu, X., Zhao, C., & Zhang, Y. (2013). Sensitivity of CAM5-simulated arctic clouds and radiation to ice nucleation parameterization. *Journal of Climate*, *26*(16), 5981–5999. https://doi.org/10.1175/JCLI-D-12-00517.1

Zhao, X., Liu, X., Lin, L., Qin, Y., Zelinka, M. D., Klein, S. A., et al. (2024). Larger cloud liquid water enhances both aerosol indirect forcing and cloud radiative feedback in two Earth system models. *Geophysical Research Letters*, *51*(2), e2023GL105529. https://doi.org/10.1029/2023GL105529

Zhu, J., & Poulsen, C. J. (2020). On the increase of climate sensitivity and cloud feedback with warming in the community atmosphere models. *Geophysical Research Letters*, *47*(18), e2020GL089143. https://doi.org/10.1029/2020GL089143

Zhu, J., Poulsen, C. J., & Tierney, J. E. (2019). Simulation of Eocene extreme warmth and high climate sensitivity through cloud feedbacks. *Science Advances*, *5*(9), eaax1874. https://doi.org/10.1126/sciadv.aax1874